Mario R. Eden, John D. Siirola and Gavin P. Towler (Editors) Proceedings of the 8th International Conference on Foundations of Computer-Aided Process Design – FOCAPD 2014
July 13-17, 2014, Cle Elum, Washington, USA

Modeling and Simulating Electrochemical Reduction of CO_2 in a Microfluidic Cell

Kunna Wu[a,b], Erik Birgersson[a], Paul J.A. Kenis[b] and Iftekhar A. Karimi[a*]

[a] *Department of Chemical and Biomolecular Engineering, National University of Singapore, Singapore, 117585*
[b] *Department of Chemical and Biomolecular Engineering, University of Illinois ar Urbana-Champaign, Urbana, Illinois 61891, United States*
cheiak@nue.edu.sg

Abstract

A steady-state, isothermal model has been presented for the electrochemical reduction of CO_2 to CO in a microfluidic cell. The model integrates the transports of charge, mass, and momentum with electrochemistry. After validation using experimental polarization curves, extensive simulations reveal a trade-off between the two performance measures: current density and CO_2 conversion. A more negative overpotential at the cathode increases the partial current density for CO_2 reduction, but decreases the Faradaic efficiency. As feed CO_2 concentration or flow rate increase, the current density and faradaic efficiency increase, but CO_2 conversion decreases slightly. A longer channel improves CO_2 conversion, but at the cost of Faradaic efficiency and current density.

Keywords: Carbon dioxide; Electrochemical reduction; Microfluidics; Modeling.

1. Introduction

Diminishing supplies of conventional energy sources and growing concern over greenhouse gas emissions present significant challenges to the world's rapidly increasing demand for energy. The electrochemical reduction of carbon dioxide has the potential to store power from intermittent energy sources such as wind, solar, and hydroelectricity in a chemical form via chemical fuels and feedstocks such as formic acid and CO (Jhong, Ma, & Kenis, 2013). When combined with a renewable source, this technology also provides a means to reduce CO_2 emissions. The majority of existing studies on electrochemical conversion of CO_2 are experimental in nature, focusing on the possible mechanisms for the many products of CO_2 electroreduction, or exploring different types of electrodes and catalysts to improve performance (Hori, 2010; Jhong et al., 2013). First-principles modeling of electrochemical microreactors can complement the current experimental work by elucidating the complex transport and electrochemistry particularly in porous electrodes, and help in designing and optimizing such reactors.

Li and Oloman (2007) first presented a crude cathode model for the electroreduction of CO_2 to potassium formate in a continuous "trickle-bed" reactor. Delacourt and Newman (2010) proposed a detailed model for CO_2 reduction to CO in a cell similar to a proton-exchange-membrane fuel cell but with an additional aqueous buffer layer. Ni (2012) and Xie & Xue (2012) also modeled CO_2 electroreduction in a solid oxide electrolysis cell. However, the present literature is lacking a detailed mathematical model of a

microfluidic electrochemical cell for the aqueous electrochemical reduction of CO_2, which has been demonstrated to be an effective reactor and a versatile analytical tool (Whipple, Finke, & Kenis, 2010). Though Wang and his coworkers (2013) have developed a model for CO_2 electroreduction to formate in a microfluidic cell, their computational approach for simulating the electrode-electrolyte interface is rather obscure, and potential distribution and the definition of overpotential are oversimplified.

We propose a steady-state isothermal model for an electrochemical microfluidic cell to reduce CO_2 to CO. The model is calibrated and validated using experimental data, and the sensitivity of several design and operating variables is analysed via simulations.

2. Mathematical Formulation

Consider the microfluidic electrochemical cell of Figure 1, which is equipped with parallel, rectangular, multi-layered channels and operates in a co-flow mode. A mixture of N_2 and CO_2 enters the cathode gas channel, while the anode is open to the atmosphere. An aqueous KCl electrolyte flows between two gas diffusion electrodes (GDEs). The cathode is coated with Ag catalyst, while the anode is coated with Pt blank at the electrode-electrolyte interface. A graphite current collector backs each GDE at the other side.

As we supply electricity to this microfluidic cell, CO_2 reduces to CO and water reduces to H_2 via reactions (1) and (2) at the cathode-electrolyte interface. The hydroxide ions produced from water splitting migrate to the electrolyte-anode interface, and get oxidised to O_2 via reaction (3).

$$CO_2 + H_2O + 2e^- \rightarrow CO + 2OH^- \quad (1)$$

$$2H_2O + 2e^- \rightarrow H_2 + 2OH^- \quad (2)$$

$$2OH^- \rightarrow 1/2\,O_2 + H_2O + 2e^- \quad (3)$$

We make the following assumptions and simplifications.

1) The system is isothermal and at steady-state. This is a reasonable assumption for an electrochemical cell with a flowing electrolyte.
2) The electrolyte is an incompressible Newtonian fluid and the flow is laminar.
3) Gas is weakly compressible and the flow in the gas channel is laminar.
4) The side walls of the cell are impermeable and the slip is zero.
5) Concentrations do not vary along the cell cross section, as we enforce slip and zero species flux at the left and right walls of the cell.

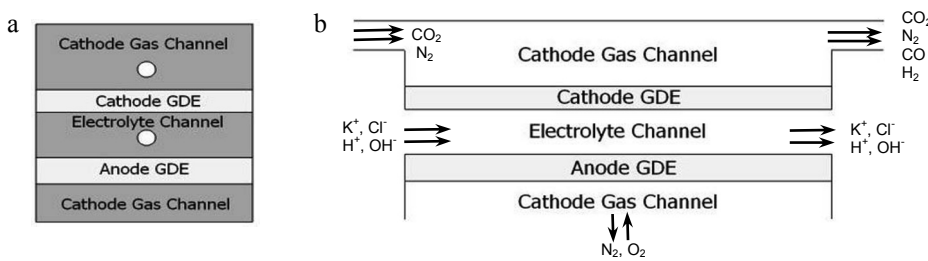

Figure 1. Schematics of (a) the front and (b) the side view of the microfluidic electrochemical cell

We consider transport in the gas channels, porous GDEs, and the electrolyte; material balance in the gas phase (cathode: CO_2, N_2, CO and H_2; anode: O_2 and N_2) and electrolyte phase (H^+, OH^-, K^+ and Cl^-); the electronic and ionic charge balance; and charge transfer kinetics. This gives us the following conservation equations

$$\nabla \cdot (\rho \mathbf{u}) = 0 \tag{4}$$

$$\nabla p = \begin{cases} -\rho \mathbf{u} \cdot \nabla \mathbf{u} + \nabla \cdot \left(\mu(\nabla \mathbf{u} + (\nabla \mathbf{u})^T) - \frac{2}{3} \mu(\nabla \cdot \mathbf{u}) \mathbf{I} \right) & \text{(Gas Channel)} \\ \frac{\rho}{\varepsilon} \left((\mathbf{u} \cdot \nabla) \frac{\mathbf{u}}{\varepsilon} \right) + \nabla \cdot \left[\frac{1}{\varepsilon} \left(\mu(\nabla \mathbf{u} + (\nabla \mathbf{u})^T) - \frac{2}{3} \mu(\nabla \cdot \mathbf{u}) \mathbf{I} \right) \right] - \left(\frac{\mu}{\kappa} \right) \mathbf{u} & \text{(GDE)} \\ -\rho \mathbf{u} \cdot \nabla \mathbf{u} + \mu \nabla^2 \mathbf{u} + \rho \mathbf{g} & \text{(Electrolyte)} \end{cases} \tag{5}$$

$$\nabla \cdot \boldsymbol{n}_i = 0 \tag{6}$$

$$\nabla \cdot \mathbf{i} = 0 \tag{7}$$

We account for diffusion and convection in the cathode, but only diffusion in the anode due to the open boundary. In the electrolyte, we consider convection, diffusion, and the migration of charge species. Then, the molar fluxes of the various species are as follows,

$$\boldsymbol{n}_i = \begin{cases} -\rho D_i \nabla \omega_i + (\rho \mathbf{u} \omega_i) & (\text{Cathode: i} = CO_2, CO, H_2) \\ -\rho D_i \nabla \omega_i & (\text{Anode: i} = O_2) \\ -D_i \nabla C_i - z_i u_{m,i} C_i \nabla \phi_l + C_i \mathbf{u} & (\text{Electrolyte: i} = H^+, OH^-, Cl^-) \end{cases} \tag{8}$$

We define the current densities at the electrodes and in the electrolyte as:

$$\mathbf{i} = \begin{cases} -\sigma_s \nabla \phi_s & \text{(GDEs)} \\ F \sum_i z_i \left(-D_i \nabla C_i - z_i u_{m,i} C_i \nabla \phi_l \right) & (\text{Electrolyte: i} = H^+, OH^-, K^+, Cl^-) \end{cases} \tag{9}$$

The electrokinetics associated with reactions (1) depends on CO_2 concentration while that for reaction (2) and (3) are assumed be mass-transport-independent.

$$i_{CO} = 2F k_{CO} C_{CO_2} \exp\left(-\frac{2\alpha_{CO} F}{RT} \eta_{CO} \right) \tag{10}$$

$$i_{H_2} = i_{H_2}^{ref} \exp\left(-\frac{2\alpha_{H_2} F}{RT} \eta_{H_2} \right) \tag{11}$$

$$i_{O_2} = i_{O_2}^{ref} \exp\left(\frac{2\alpha_{O_2} F}{RT} \eta_{O_2} \right) \tag{12}$$

The overpotentials of various species at the triple-phase-boundaries are given by the difference between the driving potential difference and the reversible potential of the half-cell

$$\eta_i = \phi_s - \phi_l - E_i \quad (\text{i} = CO, H_2, O_2) \tag{13}$$

For boundary conditions, we enforce constant compositions and flow rates at the inlets; constant reference pressure and no diffusive species fluxes at outlets; no slip and no flux at the cathode gas channel walls; charge insulation and zero slip at the vertical walls of the GDEs; constant potentials at the electrode/gas channel interface; and molar fluxes and current densities at the electrode/electrolyte interfaces.

We implemented the above model in COMSOL, with base case parameter values shown in Table 1, and solved using the finite element method. We used coordinate search method to minimize the sum of squared difference between simulated and experimental partial current densities to find the best-fit kinetic parameter values.

3. Calibration and Validation

The electrokinetic parameters in Eq. (10) to Eq. (12) are system specific, so we first fit these parameters using experimental polarization curve. The fitted kinetic parameter values are reported in Table 1. Figure 2 compares the experimentally measured current densities with the model predictions. The computed partial current densities agree well with the experimental results.

Table 1. Key parameters used in base case simulation

Parameter	Value
Operating temperature, T (K)	298
Operating pressure, p (atm)	1.0
Channel length, L (cm)	5.5
Channel width, W (cm)	2.5
Gas channel/electrode/electrolyte thickness, H_g / H_{gde} / H_{elec} (cm)	1.0/0.03/0.15
Electrode porosity, ε	0.663
Electrode permeability, κ (m^2)	2.49E-12
Inlet CO_2 / N_2 flow rate, Q_{CO2} / Q_{N2} (cm^3/min)	0.7/6.7
Inlet electrolyte flow rate (cm^3/min)	0.4
Cathode/anode applied potential, V_{cath} / V_{anode} (V)	-1.72/1.028
Fitted kinetic parameters for CO formation, k_{CO} (m/s) / α_{CO}	5.233E-8/0.107
Fitted kinetic parameters for H_2 formation, $i_{H_2}^{ref}$ (A/m^2) / α_{H2}	5.195E-7/0.200
Fitted kinetic parameters for O_2 formation, $i_{O_2}^{ref}$ (A/m^2) / α_{O2}	6.883E-7/0.456

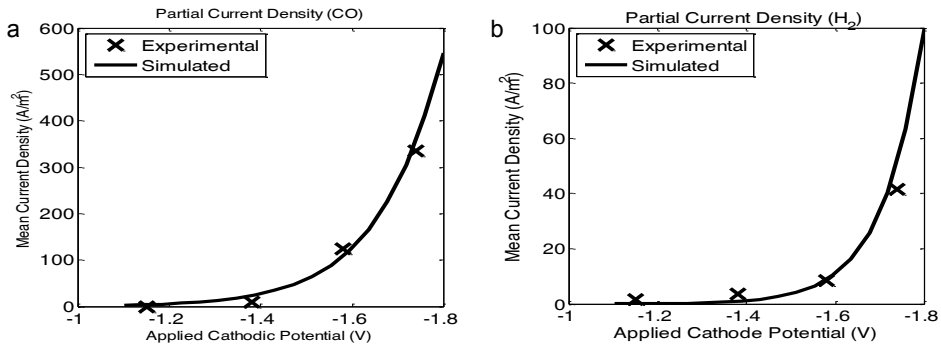

Figure 2. Comparison of mean partial current densities corresponding to (a) CO formation and (b) H_2 formation from numerical results and experimental data.

4. Results and Discussion

Figure 3(a) presents the simulated current-potential. An increase in the negative potential at the cathode increases the current densities for both CO and H_2 formations. The side reaction of H_2 formation does not show a significant effect on the total current density, until the applied potential exceeds -0.70 V (vs. AgCl) at pH 7. At high negative potentials, H_2 production rate increases much faster than CO, leading to a decrease in the Faradaic efficiency. Thus, if CO is the only desired product, then an intermediate potential should be applied. However, for syngas production, a suitable potential should be chosen to obtain the required CO to H_2 ratio.

Figure 3(b) shows the effects of CO_2 concentration, gas feed rate, and channel length. As feed CO_2 concentration increases, the CO_2 concentration at the reaction interface also increases. This leads to an increase in current density and Faradaic efficiency. This confirms that the reaction kinetics for CO_2 reduction depends on CO_2 concentration at the triple-phase boundary. However, it is noticed that the overall conversion decreases with increasing feed CO_2 concentration. In the other words, GDEs that allow faster transport of CO_2 to the reacting interface is very critical in improving current density, Faradaic efficiency and CO_2 conversion.

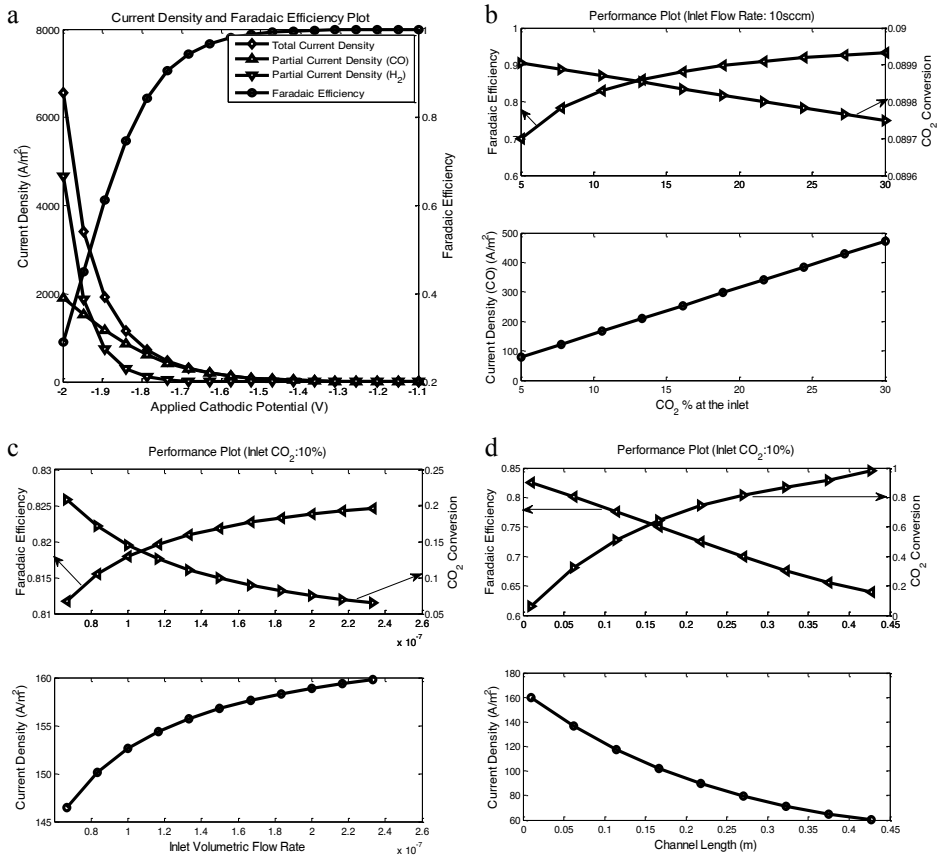

Figure 3. Effects of (a) applied cathode potential, (b) CO_2 concentration in the feed, (c) inlet gas flow rate and (d) channel length on cell performance

Initial change in the inlet gas flow rate has similar effect as increase in feed CO_2 concentration. As shown in Figure 3(c), with a faster flow rate, more CO_2 accumulating on the reaction interface and thus faster rate of reaction and larger current density. The increase in gas flow rate results in a shorter residence time in the reactor, and therefore a decrease in conversion. However, when the volumetric flow rate exceeds 0.23 cm^3/s with 10% CO_2 in the feed, further increase in flow rate has negligible effect. This may be because accumulated CO_2 at the reacting interface has been in excess for reaction, and reaction kinetics for CO_2 reduction no longer depends on surface concentration of CO_2.

Figure 3(d) shows that a longer channel length increases CO_2 conversion, but decreases Faradaic efficiency and current density. A longer channel allows more residence time, thus improves CO_2 conversion. However, the lower average CO_2 concentration in the cell reduces the current density. If CO_2 conversion is specified, we can use this model to determine the optimal channel length.

5. Conclusions

We presented a first-principles electrochemical model for CO_2 reduction to CO in a microfluidic cell. It accounts for all the significant physics and electrochemistry in the cell such as the transport of species and charges, momentum and mass conservations, and electrochemical reactions. At present, model solution requires about 30 s using 1 GB of virtual memory. Simulation results successfully predict the experimental data after the fitting of unknown parameters. It also reveals the importance of improving CO_2 transport in the GDEs, the limiting effect of feed CO_2 concentration, feed flow rate and channel length. Our model provides a basis for design and optimization, and can be suitably extended for stack design and optimization.

References

Delacourt, Charles, & Newman, John. (2010). Mathematical Modeling of CO2 Reduction to CO in Aqueous Electrolytes II. *Journal of The Electrochemical Society, 157*(12), B1911.

Hori, Y. (2010). CO_2 - reduction, catalyzed by metal electrodes *Handbook of Fuel Cells*: John Wileys & Sons.

Jhong, Huei-Ru "Molly", Ma, Sichao, & Kenis, Paul J. A. (2013). Electrochemical conversion of CO2 to useful chemicals: current status, remaining challenges, and future opportunities. *Current Opinion in Chemical Engineering, 2*(2), 191-199. doi: 10.1016/j.coche.2013.03.005

Li, Hui, & Oloman, Colin. (2007). Development of a continuous reactor for the electro-reduction of carbon dioxide to formate – Part 2: Scale-up. *Journal of Applied Electrochemistry, 37*(10), 1107-1117. doi: 10.1007/s10800-007-9371-8

Ni, Meng. (2012). An electrochemical model for syngas production by co-electrolysis of H2O and CO2. *Journal of Power Sources, 202*, 209-216. doi: 10.1016/j.jpowsour.2011.11.080

Wang, Huizhi, Leung, Dennis Y. C., & Xuan, Jin. (2013). Modeling of a microfluidic electrochemical cell for CO2 utilization and fuel production. *Applied Energy, 102*, 1057-1062.

Whipple, Devin T., Finke, Eryn C., & Kenis, Paul J. A. (2010). Microfluidic Reactor for the Electrochemical Reduction of Carbon Dioxide: The Effect of pH. *Electrochemical and Solid-State Letters, 13*(9), B109. doi: 10.1149/1.3456590

Xie, Yuanyuan, & Xue, Xingjian. (2012). Modeling of solid oxide electrolysis cell for syngas generation with detailed surface chemistry. *Solid State Ionics, 224*, 64-73.